Nanoscale

Accepted Manuscript

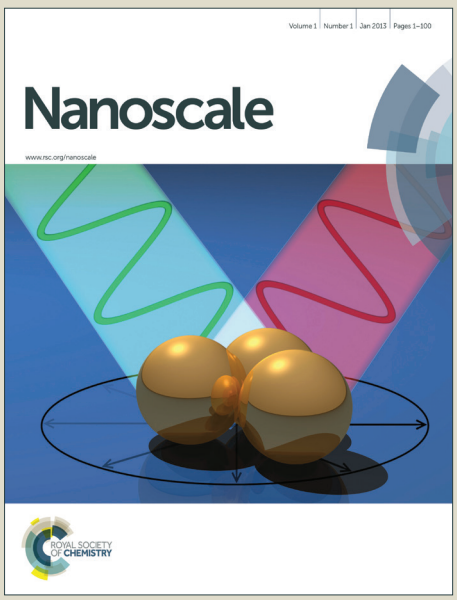

ROYAL SOCIETY OF CHEMISTRY

www.rsc.org/nanoscale

Cite this: DOI: 10.1039/c0xx00000x

www.rsc.org/xxxxxx

ARTICLE TYPE

Emission Tunable, Cyto/Hemocompatible, Near-IR-Emitting Ag_2S Quantum Dots by Aqueous Decomposition of DMSA

Ibrahim Hocaoglu,[a] Fatma Demir,[a] Ozgur Birer,[a,b,c] Alper Kiraz,[a,d] Chantal Sevrin,[e] Christian Grandfils,[e] and Havva Yagci Acar*[,a,b,c]

Received (in XXX, XXX) XthXXXXXXXXX 20XX, Accepted Xth XXXXXXXXX 20XX

DOI: 10.1039/b000000x

Size tunable aqueous Ag_2S quantum dots emitting in the near-infrared region was synthesized through decomposition of meso-2,3-dimercaptosuccinic acid (DMSA) in water. Resulting NIR QDs are highly cyto- and hemocompatible, have quantum yields as high as 6.5% and are effective optical imaging agents based on in vitro evaluations.

Introduction

Size and emission tunability, broad absorption and narrow emission properties of quantum dots (QDs) have attracted great attention for a variety of technological development as an enabler. QDs can be used in electronics, optics, energy and biomedical applications for their versatile properties. Cadmium-based semiconductor nanoparticles (CdX, X: S, Se, Te) are the most widely studied quantum dots emitting in the visible region (400-700 nm). Unfortunately, emission in the visible region is not practical for biological applications such as imaging/diagnostics. Quantum Dots emitting in the Near-Infrared region (NIRQD) has emerged as a response to increasing demand for more suitable QDs in biotechnology and medicine. Biological molecules or natural constituents such as hemoglobin, deoxyhemoglobin and water have intense interactions with visible monochromatic light.[1] Living tissues also have autoflorescence in the visible region. Near-Infrared (NIR) region between 700-900 nm where absorption and scattering activities are lower in the living tissues, defined as the therapeutic window.[1, 2]

The most frequently used NIRQDs are Cd-based, such as CdTeS, CdHgTe/CdS[3] and CdSe/CdTe[4] and there are few examples to their bio-applications.[5, 6] For example, Prasad et al. showed imaging of panc-1-tumor using functionalized CdTe/ZnS QDs.[7] CdMnTe/Hg QDs were used as an angiographic contrast agent by Morgan et al.[8] and CdTe/CdS QDs were used in the in vitro cell and in vivo tumor imaging.[9] However, heavy metal toxicity is an important concern for both *in vitro* and *in vivo* studies.[10] Recent efforts are directed towards development of Cd, Pb and Hg free, biocompatible QDs. From this perspective, silver chalcogenide quantum dots with a band gap of 0.9 eV and superior biocompatibility over Cd-based QDs are excellent candidates for bio-applications. There are two recent studies on the evaluation of cytotoxicity, cell proliferation, ROS generation, apoptosis, necrosis and DNA damages of Ag_2S QDs and both of them reported high biocompatibility.[11, 12]

Most of the Ag_2X (X: S, Se, Te) NIRQDs in literature have been prepared in organic medium using organic soluble coating materials. [13-16] Those quantum dots have emission characteristics in the 650-1200 nm range with very low photoluminescence quantum yield (below 2%).[15, 16] Alternatively, Zhu et al synthesized Ag_2S nanoparticles in ethyleneglycol at above 140 °C by the decomposition of 3-mercaptopropionic acid and transfered resulting particles into water phase without any ligand exchange procedure.[17]

There are also few examples of Ag_2S NIRQDs prepared in aqueous media. Remya et al prepared aqueous Ag_2S nano-clusters in two steps through hydrothermal decomposition of the gluthathione complex of Ag nanoparticles at low temperature over 24h.[18] Castanon et al. reported aq. synthesis of Ag_2S nanoparticles larger than 30 nm without any emission data.[19] Hocaoglu et al. have recently demonstrated a simpler, single-step synthesis of cytocompatible Ag_2S-2MPA NIRQDs via direct addition of sulphur source to silver salt in water.[20] These NIRQDs have high QYs compared to those reported in the literature but failed to produce particles luminescing at significantly different wavelengths along with good QY. Common approach towards manipulating size is the adjustment of reaction time, ligand/Ag or Ag/S ratio which usually failed in case of Ag_2S.[12, 20] Recently, Yang et al reported Ag_2S-BSA QDs with emission between 1050-1295 nm through Ag/S ratio variation.[21] Glutathione stabilized Ag_2S QDs were prepared (960-1050 nm) with 0.96-1.97% QY (reference: indocyanine green, QY 13%).[22] Most recently, Gui et al reported size tunable (687-1096 nm) Ag_2S QDs prepared with poly (acrylic acid)-graft-cysteamine-graft-ethylenediamine coating with QY 14-16% (reference: indocyanine green).[23]

We have previously demonstrated that meso-2,3-dimercaptosuccinic acid (DMSA) can be used as a slow sulphur releasing agent between pH 7-10 and at temperatures between 50-90 ºC.[24] Size tunable CdS QDs were synthesized by the decomposition of DMSA and the best condition for effective size tuning was determined as pH 7.5 and 70 °C.[24] In such reactions, DMSA acted both as a sulphur source and a coating material. Furthermore, DMSA is a metal chelating agent[25] and an FDA approved drug used in heavy metal poisoning.[26] DMSA coating improved the cytocompatability of CdS QDs significantly.

In this article, DMSA is evaluated as a slow S-releasing reagent and a biocompatible coating material in an effort to synthesize biocompatible, size tunable Ag_2S NIR QDs in a very simple procedure. At mole ratios of DMSA/Ag of 1.5, 2.5 and 3.5 particles with emission maximum between 730-860 nm with QYs as high as 6.5% were achieved at 70°C within 5h. In vitro assessment of cytocompatibility and hemocompatibility were performed for these Ag_2S/DMSA NIRQDs. Cytotoxicity of QDs are frequently determined, however, till now, very few studies have examined the hemocompatibility of QDs.[27-29] Indeed, when diluted in the blood stream, nanomaterials will be able to elicit several toxicological reactions, in particular: embolisation, hemolysis, cellular activation, but also several well-known biological cascades such as coagulation, complement activation, kinin/kininogen, fibrinolysis. Moreover, it is important to stress that the first barrier that nanoparticles encounter is the blood itself and the Reticulo-Endothelial System (RES). Because of the high efficiency of this clearance system in eliminating foreign bodies from the blood circulation, blood life-time of nanopartices does not exceed typically seconds/minutes. Therefore, in addition to cytocompatability, assessment of hemocompatibility is essential before considering any preclinical studies. Compared to macroscopic particles, hemoreactivity of nanoparticles may be expected to be significantly enhanced due to very high surface/volume ratio. Therefore, a significant interaction of nanoparticles with humoral and cellular blood components of the blood is highly expectable.

These Ag_2S/DMSA NIRQDs are non-toxic up to 200 µg/ml in HeLa cancer cell lines and showed only 20% reduction in cell viability of 3T3 NIH cells in 24h. Hemocompatibility testing has also highlighted that they do not elicit any major reaction within the blood up to a concentration of 100 µg/mL. They have provided efficient cytoplasmic labelling of HeLa cells demonstrating great ability for optical imaging.

Materials and Methods

Materials

All reagents were analytical grade or highest purity. Meso-2,3-dimercaptosuccinic acid (DMSA) and silver nitrate ($AgNO_3$) were purchased from Sigma-Aldrich. Sodium sulfide (Na_2S) was purchased from Alfa-Aesar. Sodium hydroxide (NaOH), 2-Mercaptopropionic acid (2-MPA), ethanol and aceticacid (CH_3COOH) were purchased from Merck. LDS 798 Near-IR laser dye was purchased from Exciton Inc. Only Milli-Q water (18.2 MOhm) was used when needed. For biological applications, DMEM medium (with 4500 mg/L glucose, 4.0 mM L-glutamine, and 110 mg/L sodium pyruvate), trypsin-EDTA, penicillin-streptomycin and fetal bovine serum were purchased from HyClone, USA. Thiazolyl blue tetrazolium bromide (MTT) *Biochemica* was purchased from AppliChem, Germany. Paraformaldehyde solution 4 % in PBS and UltraCruz™ 96 well plates were purchased from Santa Cruz Biotechnology, Inc., USA. Glass bottom dishes were purchased from MadTek, USA. Dimethyl sulfoxide Hybri-Max™ and phosphate buffered saline (pH 7.4) were purchased from Sigma, USA.

Preparation of Ag_2S Nanoparticles

As an example, 42.5 mg of $AgNO_3$ was dissolved in 75 ml of deoxygenated deionized water. 25 ml of deoxygenated aqueous DMSA solution prepared at pH 7.5 was then added to the reaction mixture. pH of the solution was adjusted to 7.5 by using NaOH and CH_3COOH solutions (2M). Under vigorous mechanical stirring at 5000 rpm, reaction mixture was brought to the desired temperature (70 or 90 ^oC). During the reaction, samples were taken at different time points to follow the particle growth. Prepared quantum dot solutions were washed with DI water using Amicon-Ultra centrifugal filters (3000 Da cut off) and stored in dark at 4 ^oC.

Influence of reaction variables were studied in different reactions keeping the Ag concentration fixed at 2.5mM and varying DMSA concentrations to achieve DMSA/Ag ratio of 1.5, 2.5 and 3.5 (Table 1&2).

Cell Culture

Human cervical carcinoma (HeLa) and mouse fibroblast cells (NIH-3T3) were cultured according to ATCC recommendations. Cells were cultured in DMEM medium with 4500 mg/L glucose, 4.0 mM L-glutamine, and 110 mg/L sodium pyruvate. Complete medium also contained 10% fetal bovine serum and 1% penicillin-streptomycin antibiotic solution. Trypsin-EDTA was used for cell detachment and cells were incubated 37 ^oC under 5% CO_2.

Determination of Cytotoxicity

Cytotoxicity was evaluated by performing thiazolyl blue tetrazolium bromide (3-(4,5-dimethyl-thiazol-2yl)-2,5-diphenyltetrazolium bromide, MTT) assay on HeLa and NIH-3T3 cells. 96-well culture plates were seeded with 10^4 cells in culture medium and incubated at 37 ^oC and 5% CO_2 for 24 h. Following incubation, medium was replenished; cells were treated with QDs (10 to 150 µg/mL) and incubated for 24 h. After washing, MTT reaction solution was added on the cells and incubated for 4 h. DMSO:Ethanol (1:1) solution (100 µL) was added with gentle shaking for 15 min to dissolve the purple formazan. Absorbance at 600 and 630 nm was measured with an ELISA analyzer and reference absorbance at 630 nm was subtracted from the absorbance at 600 nm. Experiments were repeated for four times. Absorbance values of the QDs were substracted from the formazan values. Statistical significance of the observed differences was determined using one-way ANOVA with Tukey's multiple comparison test of GraphPad Prism software package from GraphPad Software, Inc., USA

Cell Imaging

50,000 HeLa cells were seeded in glass bottom dishes. After 18 h incubation, cells were treated with 150 µg/mL QDs in full medium for 6 h. After being washed with PBS (pH 7.4), cells were fixed with 4% paraformaldehyde for 15 min and wash step was repeated.

A home-built sample scanning confocal microscope based on an inverted microscope frame (Nikon TE 2000U) equipped with a 60X (Nikon, NA=1.49) oil immersion objective was used for image acquisition. Excitation wavelength was 532 nm. A broadband 10/90 dichroic beam splitter was used for excitation. A long pass glass filter (RG665) was placed before Silicon APD based photon counting modules to detect the QD emission.

Hemocompatibility Studies

Hemocompatability tests were performed with a Ag_2S NIRQD which was synthesized at DMSA/Ag ratio of 2.5, 70°C in 4h. Hemocompatibility tests were performed according to ISO standards (10993–4). Normal human blood from healthy volunteer donors was collected in Terumo Venosafe citrated tubes (Terumo Europe N. V., Belgium). Experiments were done within 2 h after blood collection. All tests were performed with the agreement of the local ethical committee of the Medicine Faculty of the University of Liège. Hemocompatibility of Ag_2S/DMSA NIRQDs was evaluated by studying hemolysis, morphology of blood cells, complement activation (C3a), and coagulation activation, both through the extrinsic pathway (PT assay) and the intrinsic pathway (APTT assay). QDs dispersed in PBS were diluted in whole blood in order to obtain final nanoparticle concentrations of 100, 10, and 1 µg/mL. Samples were incubated for 15 min at 37 °C under lateral agitation (250 rpm).

Micrographs of blood smear

After blood incubation, 5 µL of the blood was withdrawn and spread on a microscopy glass slide. Blood cells were observed with an Olympus Provis microscope at 20× and 50× magnification in transmission mode.

Haemolysis

The haemolytic test was performed following Standard Practice for Assessment of Haemolytic Properties of Materials (ASTM designation F 756-00). Briefly, after QD incubation in whole blood, the samples were centrifuged at 600g for 5 min at room temperature, and supernatants were collected and mixed with the cyanmethemoglobin reagent. The hemoglobin released was measured by reading the absorbance of 100-fold dilution of whole blood in Drabkin's reagent at 540 nm in a microplate reader (Anthos HT III, type 12600, Anthos, Salzburg, AU). A calibration curve was established using bovine hemoglobin as the standard. Saponine (0.8 mg mL^{-1}) and PBS were used as positive and negative controls, respectively. Hemolysis was expressed as the percentage of hemoglobin released to total hemoglobin content, taking the positive control as 100% of hemolysis. The tests were done in triplicate.

Count and size distribution of RBCs, platelets and white blood cells

QD dispersions and blood were prepared and incubated as described before. After 15 min of incubation, blood cells were counted and their size distribution was determined with CELL-DYN 18 Emerald (Abbott Diagnostics). Three analyses were conducted per sample.

Complement Activation

Complement activation was assessed using the Human C3a ELISA kit for quantification of Human C3a-des-Arg (Becton Dickinson). After a 15 min incubation of blood and QD mixtures, EDTA (1 mM final) was added to block any future complement activation. Samples were centrifuged at 2000g for 5 min at rt, and supernatants were used for the analysis of complement activation following the kit protocol (BD OptEIA, Human C3a ELISA, Cat. No.550499). Absorbance was measured at 450 nm with a microplate reader (Anthos HT III, type 12600). Plasma containing 2 mg mL^{-1} of Zymosan was taken as a positive control and plasma without additives as a negative control. The concentration of C3a was expressed as a percentage of activation by reference to the negative control set at a value of 100% of complement activation. Measurements were done in duplicate.

Coagulation Experiments

Whole blood and QD dispersions were mixed and incubated as described before. Samples were centrifuged at 2000g for 5 min at rt, and the supernatants were collected, recalcified to reverse the effect of citrate anticoagulant, and supplied with the specific activators of coagulation (thromboplastin). Prothrombin time (PT) to evaluate the extrinsic pathway, and activated partial thromboplastin time (APTT) to evaluate the intrinsic pathway, were measured directly with a Dade Behring Coagulation Timer analyzer (BCT) (Siemens Healthcare Diagnostics NV/SA, Belgium) using commercial reagents (Thromborel® S, Dade Behring/Siemens, for PT determination and C.K. PREST kit, Roche Diagnostics, France, for aPTT). Kaolin reagent was used as a positive control and PBS as a negative control. Clotting time was measured for each sample, and coagulation capacity was expressed as a percentage, taking the value of standard human plasma (Dade Behring/Siemens) as 100%. Measurements were done in duplicate.

Characterization Methods

A Shimadzu 3101 PC UV-Vis-NIR spectrometer was utilized for the absorbance spectroscopy in the 300-1000 nm range. The Brus equation[30, 31](eqn.1) was used for the particle size calculation from experimentally determined absorption onset.

$$\Delta E = \frac{\hbar^2\pi^2}{8R^2}\left[\frac{1}{m_e}+\frac{1}{m_h}\right] - 1.8\frac{e^2}{\varepsilon_{Ag_2S}4\pi\varepsilon_0 R} \quad (1)$$

ΔE is the band gap energy difference between the bulk semiconductor and the quantum dot, R is the radius of quantum dot, m_e (0.286 m_0) and m_h (1.096) are the respective effective electron and hole masses for Ag_2S,[32] and ε_{Ag2S}(5.95) is the dielectric constant of bulk Ag_2S.[32]

Photoluminescence spectra were recorded with a homemade setup. The system was built around a 1/8 monochromator (Newport Cornerstone 130) equipped with a 600 l/mm grating working in 400-1000 nm range. The excitation source was the frequency doubled output of a DPSS laser at 532 nm. The luminescence signal was filtered by a 590 nm long pass filter before it was wavelength selected and detected with a Si detector with femtowatt sensitivity (Thorlabs PDF10A, 1.4 x 10^{-15} $W/Hz^{1/2}$). The power of the excitation source was monitored with a powermeter and the reported spectra are normalized for excitation power.

QY calculations were done based on the procedures detailed in the literature.[33-35] As a reference LDS 798 NIR dye (QY is 14% was reported by the producer) was used. Typically, five different concentrations of the dye (in MeOH) and sample (in water) were prepared, all with absorption below 0.15 at excitation wavelength and the PL spectra of each was obtained. Proportion of the areas under the emission peaks were used in the calculations. Area values of the different concentrations were plotted for both

samples and the reference dye (standard). Typical QY is the ratio of the slope of the sample (m_{slope}) and the slope of the dye ($m_{standard}$). The equation below is used for QY calculation (eqn 2).

$$\Phi_{yield} = \frac{m_{sample}}{m_{standard}} \left(\frac{\eta^2_{water}}{\eta^2_{MeOH}} \right) \qquad (2)$$

Refractive indices of sample (η_{water}) and the reference dye (η_{MeOH}) solutions are important for the calculation.

Samples were dried into powder form using freeze-drier for X-PS and XRD analysis. XPS analyses were performed with a Thermo Scientific K-Alpha XPS with Al K-alpha monochromatic radiation (1486.3 eV). Ag_2S powders were placed on adhesive aluminum tape and 400 μm x-ray spot size was used. The pass energy of 50.0 eV corresponds to a resolution of roughly 0.5 eV. The base pressure was below 3×10^{-9} mbar and experimental pressure was about 1×10^{-7} mbar due to charge neutralization with flood gun. C1s peak at 285.0 eV was assigned as the reference signal for evaluations.

D8 advance Bruker instrument was used for the XRD. Solid samples were put on a piece of a glass with a double sided tape. The glass was placed into sample holder with dough. Crystal peaks were recorded between 2θ angles of 10°-80° with Cu K-α radiation (λ=1.5406).

For TEM analysis, JEOL ARM 200 CFEG Cs-corrected STEM operated at 200 kV was used. EDS was done with JEOL Centurion detector with 100 mm^2 detector area.

Hydrodynamic size and the zeta potential of the aqueous colloidal Ag_2S/DMSA were measured by the Malvern zetasizer nano ZS.

Ag^+ ion concentration of the quantum dot solutions were determined by Spectro Genesis FEE Inductively Coupled Plasma Optical Emission Spectrometer (ICP OES) using appropriate regression curves created with standard solutions. QDs were etched with nitric acid and sulfuric acid mixture and diluted with DI water for the ICP analysis. Experiments were done in triplicate and the average was reported.

Results and Discussion

In a typical reaction, Ag^+ and DMSA forms a complex with a strong absorbance at around 255 nm (Fig. 1a). Absorbance maximum of the initial complex vanishes slowly with time as the reaction mixture was heated indicating the decomposition of the complex and formation of the Ag_2S crystals. As Ag_2S nanocrystals form and grow, the absorbance onset shifts to longer wavelengths (Fig. 1b).

Primary purpose of using DMSA here is to benefit from slow sulphur release from DMSA to tune the crystal size and therefore the emission wavelength of Ag_2S QDs. Therefore, DMSA/Ag ratio and the reaction temperature which influence the decomposition rate were studied as variables and their influence on the particle size, emission wavelength and quantum yield were analysed. Three different DMSA/Ag ratios were used at fixed temperature of 70 ºC and pH 7.5.

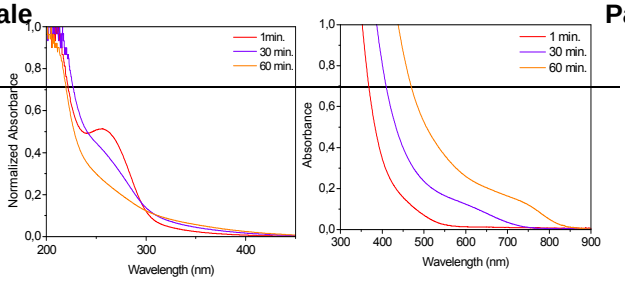

Fig. 1 Absorbance spectra of a) Ag^+-DMSA complex b) Ag_2S-DMSA NIRQDs prepared at 90 °C at DMSA/Ag= 2.5.

Initial reaction at DMSA/Ag ratio of 1.5 was monitored for 19h by the UV-Vis spectrophotometer and spectrofluorometer (Fig. 2a). Red shift of the absorbance onset implies crystal growth with time as DMSA decomposes slowly and releases sulphur. This profile is completely different than those obtained with 2MPA coating and Na_2S as a sulphur source, where only intensity changed with time. Crystal sizes of Ag_2S/DMSA QDs were increased from 2.20 to 2.95 nm with time as calculated by the Brus equation using the absorbance onsets (Table 1). The increase in crystal sizes were accompanied by the red shift in emission maximum of the particles from ca. 780 to 920 nm. Luminescence intensity of the particles continuously increased up to 4h (emission maximum at 828nm) and then decreased with further increase in particle size. Major drop in the luminescence intensity was observed at the 5th h. Yet, DMSA decomposition provided size tunable Ag_2S NIRQDs luminescing between 780-920 nm in a one pot reaction.

Table 1 Influence of DMSA/Ag ratio and reaction time on the properties of Ag_2S-DMSA NIRQDs

DMSA /Ag	Time.	λ_{cutoff} [a] (nm)	Size[b] (nm)	Band Gap (eV)	$\lambda_{em,max}$ (nm)	FWHM (nm)	QY[c] %
1.5	1h.	662	2.20	1.88	782	195	
1.5	3h	792	2.57	1.57	800	173	
1.5	4h	844	2.73	1.47	828	158	
1.5	5h	870	2.82	1.43	858	150	
1.5	19h	907	2.95	1.37	923	-	
2.5	1h.	677	2.24	1.83	730	170	
2.5	3h	791	2.60	1.57	789	129	
2.5	4h	810	2.62	1.53	810	139	6.5
2.5	5h	833	2.70	1.49	829	137	6.3
3.5	30min.	625	2.10	1.99	730	-	
3.5	2h	807	2.61	1.54	794	142	
3.5	4h	837	2.71	1.48	834	134	6.4
3.5	9h	890	2.89	1.40	910	>180	

T=70 °C pH=7.5, [a]Determined from absorbance spectrum, [b]Diameters of the particles calculated by Brus equation, [c] Quantum yield. LDS 798 NIR dye was used as a reference.

Reactions were performed at higher DMSA/Ag ratio as well to evaluate its impact on the rate of crystal growth, size tunability and luminescence efficiency. Increasing the DMSA amount impacts the reaction in two counteracting ways: Larger amounts of DMSA can reduce the particle size as it can passify the surface

of the growing crystals at an earlier stage. On the other hand, increasing the DMSA amount introduces more S^{2-} to the medium through decomposition which decreases the Ag/S ratio and increases the particle size. Absorbance and photoluminescence spectra of Ag_2S synthesized at DMSA/Ag ratio of 2.5 and 3.5 are shown in Fig.2b and 2c. As particles grow with time, a distinctive absorption feature appeared in 3h and luminescence maxima starting around 750 nm shifted towards 850 nm in 5 h. Any further reaction caused a dramatic drop in the luminescence intensity although emission maximum shifted to ca 920 nm. As the DMSA/Ag ratio increased the major impact was seen in the full with at half maximum (FWHM) as it got narrower at high ratios. Increasing DMSA amount from 1.5 to 2.5 caused a small decrease in size and blight blue shift in emission peak and increasing further to 3.5 increased the size and caused a slight red shift in the emission (Fig. Sup1). These refer to early passivation of the growing crystal with increasing coating amount, and increasing crystal size with decreasing Ag/S ratio at higher concentration of DMSA, as proposed earlier. But overall, increasing DMSA/Ag ratio did not cause a dramatic increase in particle size/emission maximum but a narrowing in the emission peak with a slight increase in luminescence intensity at the ratio of 3.5 (Fig. S1, Table S1). These indicate that at these ratios (2.5 and 3.5) excess DMSA was most influential in stabilizing the surface. At all DMSA/Ag ratios QDs produced in 4h have the highest luminescence intensity within 810-834 nm peak emission range with a QY around 6.4% with respect to LDS 798 NIR dye (14% QY in DMSO) (Table 1, Table S1) which is quite good compared to most NIR emitting QDs in the literature[21] and good enough to evaluate these particles for bio-imaging purposes as will be demonstrated later in this article.

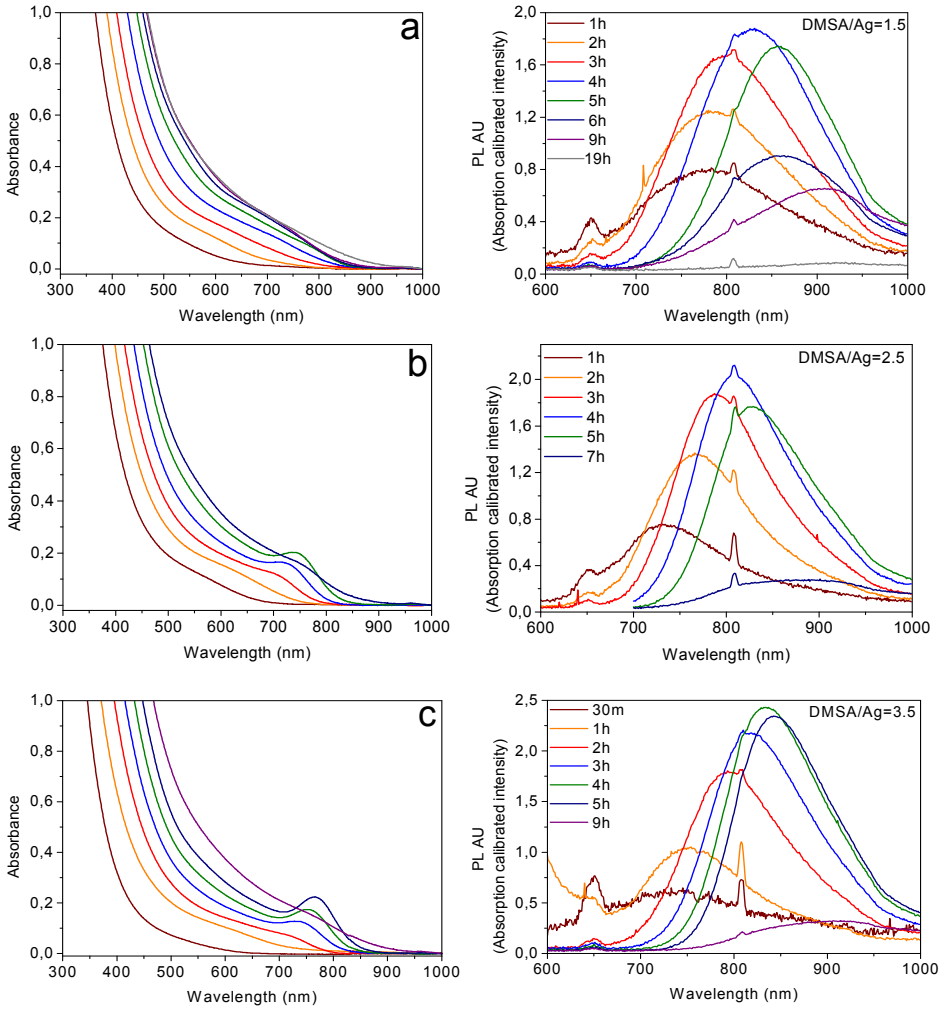

Fig. 2 Absorbance and corresponding photoluminescence spectra of Ag_2S-DMSA NIRQDs at different time points during the synthesis performed at 70 ^oC and DMSA/Ag ratios of a) 1.5 b) 2.5 c) 3.5.

One of the important parameters affecting decomposition of DMSA and particle growth is temperature. Synthesis of Ag_2S-DMSA NIRQDs (DMSA/Ag = 2.5) at 90 ^oC speeded up the sulphur release and the crystal growth. As can be seen in the absorbance spectra in Fig. 3a, particle growth stopped at the 3rd hour.

A distinct red shift in emission maximum was observed in every 30 min from 750 to 900 nm. Particles with emission maximum at

830-840nm were achieved in after 5h at 70°C but in 1h at 90°C. However, photoluminescence intensity of these particles are about four times lower than the particles synthesized at 70°C (Fig.S2).

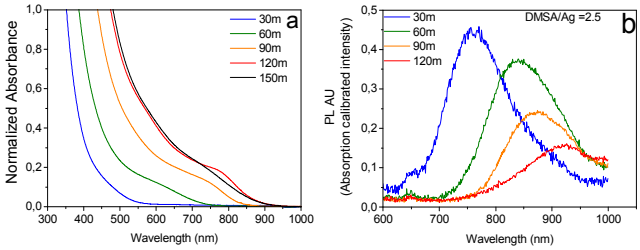

Fig. 3 Absorbance a) and PL b) spectra of the samples taken from the synthesis of Ag_2S NIRQDs at 90°C.

Table 2 Influence of the temperature on DMSA decomposition and NIRQD properties

Time (min)	λ_{cutoff} [a] (nm)	Size [b] (nm)	Band Gap (eV)	$\lambda_{em,max}$ (nm)	FWHM (nm)
30	739	2.41	1.68	760	150
60	837	2.70	1.48	840	165
90	886	2.87	1.40	875	168
120	886	2.87	1.40	926	>170

T=90 °C, DMSA/Ag=2.5, [a]Determined from absorbance spectrum, [b]Diameters of the particles calculated by Brus equation.

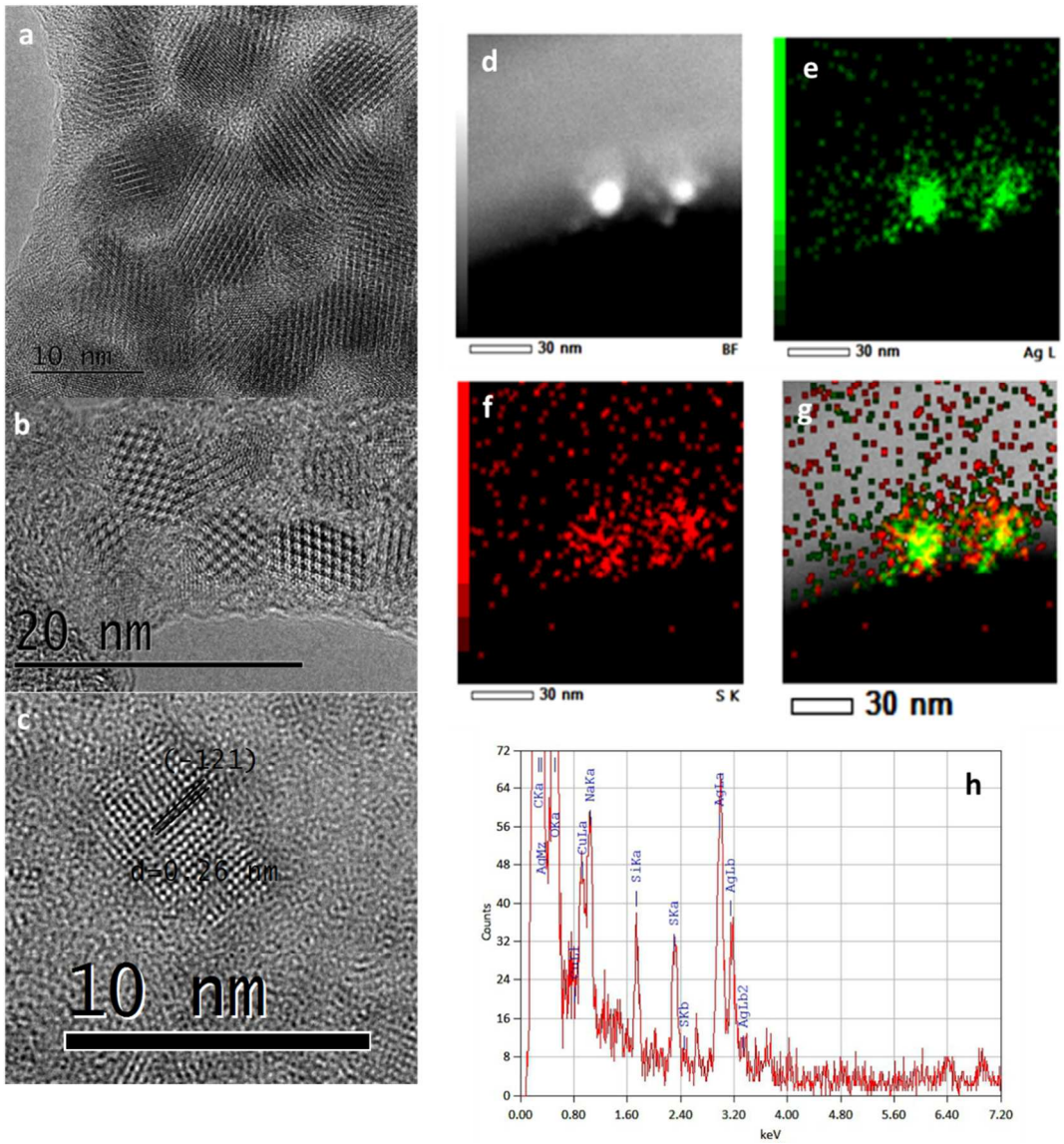

Fig. 4 TEM and EDX Analyses of the Ag_2S-DMSA NIRQDs. TEM of the nanoparticles at a) 10 nm b) 20 nm scale, c) focused lattice planes for defining d-spacing parameter corresponding plane. d) Bright field image of the Ag_2S-DMSA NIRQDs, e) Ag and f) S elemental mapping and g) their merged image showing composition of the particles. h) Ag and S transitions by EDX acquisition.

TEM images of Ag_2S-DMSA NIRQDs show mostly spherical and highly crystalline structure with particle sizes between 5-8

nm (Fig. 4a and 4b). Interplanar distance of the crystallite was measured as 0.26 nm (Fig. 4c) which is correlated with the -121 plane of the monoclinic Ag_2S in alpha phase (JCPDS: 14-0072).[36, 37] Significant movement and aggregation were observed during the measurement possibly due to the presence of organic coating. Crystal sizes measured by TEM do not correlate well with the sizes calculated by the Brus equation, but sure are more reliable. Sizes obtained from TEM are slightly smaller than sizes measured by DLS as expected which is due to the presence of the coating material (Fig. S3). Yet, sizes calculated by the Brus equation and reported in Table 1 and 2, can be used to determine the influence of reaction variables on the particle size and hence the luminescence wavelength. Although, Brus equation is used frequently for size calculation of quantum dots, there are no reports in the literature where both the size measured by TEM and calculated by the Brus equation are present for Ag_2S quantum dots. This is probably due to the significant differences in results as we observed here. None of the m_e, m_h values reported for Ag_2S provided diameters matching with those obtained from TEM. Recently, Zhang et al. reported size tunable synthesis of Ag_2S QDs through decomposition of Ag-diethyldithiocarbamate at high temperatures and measured sizes of QDs by TEM.[38] Smallest particles they have prepared have a broad luminesence centered at 975 nm with an average diameter of 2.4 nm. This is close to our largest particle diameter and luminescence peak. Yet, although not reported directly, from the available UV-absorbance data, it seems like their TEM based size analysis will not match to diameters calculated by the Brus equation either.

XPS analysis confirmed the chemical composition of the Ag_2S-DMSA NIRQDs. Binding energies (BE) and corresponding signals of Ag 3d and S 2p core level are shown on Fig. 5. Ag has peaks at the BEs of 367.73 ($3d_{5/2}$) and 373.72 ($3d_{3/2}$) eV consistent with +1 oxidation state in bulk Ag_2S.[39, 40] The sulphur 2p region is fitted to two doublet sets; the intense pair ($2p_{3/2}$ at 163.39 eV) belong to S of the coating material (DMSA). The weak pair ($2p_{3/2}$at 161.51 eV) corresponds to the bond of Ag-S-Ag originating from the inorganic core.

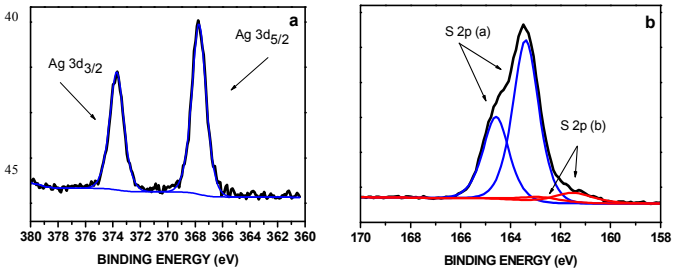

Fig. 5 XPS spectra of Ag_2S-DMSA NIRQDs. a) Ag 3d region b) S 2p region.

DMSA coated Ag_2S QDs have a typical XRD pattern seen on Fig. 6. Bulk form of Ag_2S is in alpha phase having the monoclinic crystal structure at room temperature.[37] However, Ag_2S QDs in nanoparticle form exhibits an amorphous pattern possibly due to the small size and organic coating around the inorganic core. Crystalline peaks are hidden under the amorphous peak. Annealing of QDs at 180 °C provided the typical XRD pattern matching with the monoclinic phase (JCPDS: 14-72).[15]

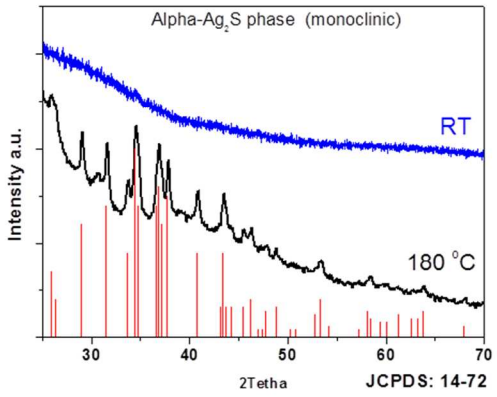

Fig. 6 XRD patterns of the Ag_2S-DMSA QDs as is (RT) and annlealed at 180 °C.

Assesment of *In Vitro* Cytotoxicity

Toxicity of quantum dots is very critical for biological applications. Ag-chalcogenites reported to exhibit almost no toxicity in different cancer cell lines.[14, 21] In case of BSA coated Ag_2S, cell proliferation was observed and this was attributed to BSA which may act as a nutrient.[41] We have shown excellent biocompatibility of 2MPA coated Ag_2S not only in cancer cell lines but also in more susceptible NIH-3T3 cells.[20] Very recently, glutathione coated Ag_2S NIR QDs were reported to have negligible cytotoxicity in HepG2 and L929 cells.[22, 42]Analysis of apoptosis and necrosis studies of Ag_2S coated with a multidentate polymer also indicated negligible cytotoxicity.[23]

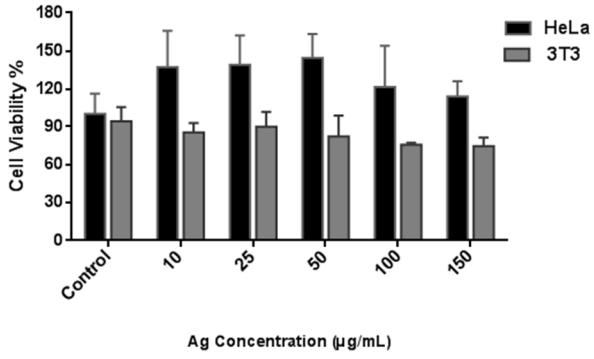

Fig. 7 Dose dependent cell viability of HeLa cancer cells and NIH/3T3 mouse fibroblast cells after 24 incubation with Ag_2S-DMSA quantum dots.

Toxicity of DMSA coated Ag_2S quantum dots to HeLa and NIH-3T3 cells were evaluated using MTT assay. In 24 h incubation, HeLa cells were not affected up to 150 µg/ml of Ag (corresponding to QD concentration of 0.84 mg/ml) (Fig. 7). Similar to our previous results with Ag_2S-2MPA and literature[41], an increase in the cell viability, possibly indicating proliferation was observed in HeLa cells. Causes of such behaviour are still not clear. NIH-3T3 fibroblast cells are more vulnerable than the cancer cell lines, thus, cell viability decreased by about 20% at

100 µg Ag/mL corresponding to 0.56 mg/ml incubation of the Ag_2S QDs which is an extremely high dose for these studies (Fig. 7). Most studies would stop at about 100µg QD/ml dose. Overall, DMSA coated Ag_2S NIRQDs are cytocompatible nanoparticles.

Hemocompatibility Assesment

Quantum dots` hemocompatibility was evaluated by studying hemolysis, the morphology of blood cells, complement activation (C3a), and coagulation activation, through the extrinsic and intrinsic pathways.

RBC integrity in the presence of QD's

The main cell population of the blood, erythrocytes, are the first to be evaluated in any hemocompatibility studies.

Hemagglutination (erythrocyte aggregation), plasma membrane rupture or changes in cell morphology are amongst the possible reactions which can occur when a foreign nanomaterial is in contact with the whole blood. All these phenomenon can induce severe circulatory disorders and even lethal toxicity. In view to exclude any possible change in RBC's, we have characterized them by adopting complementary techniques. Following blood incubation with QD's, hemolytic test was conducted according to the ASTM (Standard Practice for Assessment of Haemolytic Properties of Materials). The hemolysis rates determined in the presence of the formulations did not exceed 2% (see Table 3). Therefore these QD's may be considered non-hemolytic within the concentrations tested. This is in agreement with the hemolysis rates reported for BSA coated Ag_2S QDs at similar concentrations.[21] As a confirmation QD's under study did not affect RBC size distribution profile and cell counts (Fig. 8). The microscopic analysis of blood smear (results not showed) also demonstrates the absence of any morphology changes after blood contact with the samples. Therefore, we may conclude that these nanoparticles do not affect the integrity of erythrocytes, the blood major cellular component. This observation is not really surprising taking into account that our QD's have a relatively strong negative Zeta potential. These surface characteristics are therefore counteracting any possible ionic interaction with erythrocytes which have negative surface charges as well.[43]

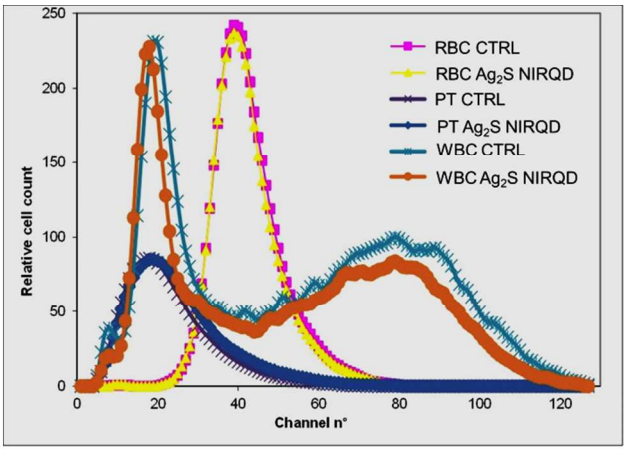

Fig. 8 Comparison of the blood cell distributions (Red blood cells (RBC's), Platelets (PT) and White Blood Cells (WBC) of the blood control to the blood incubated with Ag_2S NIRQD (100 µg/mL).

Table 3 Percentage of hemolysis, complement activation, and hemostasis activation (Quick and TCA) after incubation at 37°C of the QDs in whole blood.

QD's (µg/mL)	Hemolysis[a] (%)	Complement activation[b] (%)	Quick activation[c] (%)	TCA activation[c] (%)
1	0.08 ± 0.00	102.2 ± 6.6	93.4 ± 7.6	102.0 ± 5.2
10	0.22 ± 0.07	135.1 ± 6.3	98.4 ± 3.3	88.1 ± 6.1
100	0.22 ± 0.07	116.2 ± 1.1	100 ± 4.1	68.6 ± 4.5
Ctrl +	39.66 ± 0.07	158.9 ± 3.6	123.2 ± 3.2	-
Ctrl -	0.37 ± 0.09	100.0 ± 3.9	100 ± 4.3	100.6 ± 5.0

[a] Hemolysis percent represent free plasma hemoglobin released as a result of contact with the test material divided by the total blood hemoglobin multiplied by 100. Ctrl +: Saponin, Ctrl -: PBS. [b] Complement activation is expressed as a % of C3a concentration, adopting normal blood incubated in the same conditions as 100%. Ctrl +: blood incubated with Zymosan, Ctrl -: Plasma with no additives. [c] Quick and TCA hemostasis assays are reported in % of the clotting ability of the sample compared to the clotting ability of a standard human plasma normalized to 100. Ctrl +: Kaolin, Ctrl - : PBS.

Platelets and White Blood Cells (WBC's) behavior in the presence of QDs

Platelets, the second main cell population of the blood, are by far more reactive to the presence of foreign surfaces compared to RBC's. Indeed one of their primary functions in hemostasis relies upon their rapid adhesion to the foreign surface exposed by an injured vessel in order to limit any bleeding. Platelet plasma membrane is particularly rich in various biological receptors and are also well-known to interact with various synthetic surfaces,

including those in nano-size range.[44] As part of our immune system, some of our WBC's, in particular neutrophils and monocytes have to interact quickly with foreign materials in order to clear them from the blood compartment.

The comparison of the platelet and leucocyte size distribution of the blood control to the blood contacted with QDs (Fig. 8) clearly highlights that at the highest concentration of nanoparticles assessed, 100 µg/mL, no significant alteration is observed for any cell type. It is also the case for the global counting of these cells (results not shown). At a level of our pre-screening hemocompatibility study, these data are therefore supporting the fact that Ag_2S-DMSA NIRQDs do not interact significantly with the various blood cell elements. This observation is of particular interest regarding platelets which are well-known to react when in contact with foreign body surfaces.

The complement system is also part of our immune response to facilitate the elimination of certain pathogens from the body. But its chronic activation throughout the alternative pathway, via the nonspecific adsorption to foreign surface and cleavage of the C3 protein to produce C3a, can be responsible for hypersensitivity and anaphylaxis reactions.[45] Complement activation mediated by nanoparticles can also result in their rapid removal from systemic circulation by mononuclear cells via a receptor-mediated phagocytosis of complement. Based on the data provided on Table 3, only a slight activation of the complement system, which is not dose dependent in the range of QD concentrations tested, was detected.

Assessment of hemostasis in the presence of Ag_2S-DMSA QDs

The effect on hemostasis control was determined by coagulation assays, both through the extrinsic pathway (PT assay) and the intrinsic pathway (APTT assay). Clot formation was determined after blood incubation with QDs. Clotting ability of the standard plasma is assumed to be 100%. The longer it takes plasma to clot, the lower is its clotting ability, and the lower is the resulting test value expressed in percent to the standard plasma. It is also worth mentioning that these two coagulation pathways are intrinsically linked. For example, tissue factor–factor VIIa complex initiating the extrinsic pathway is also capable of activation of factor IX of the intrinsic pathway; in turn, the intrinsic tenase complex influences the tissue factor-dependent pathway.[46] The extrinsic coagulation pathway was not affected by Ag_2S/DMSA NIRQDs, while the intrinsic pathway was significantly inhibited at the highest concentrations of the QDs (100 µg/mL) (Table 3). As reported recently, inhibition of intrinsic and extrinsic pathways of coagulation can be explained by the non-specific adsorption of proteins involved in the coagulation cascades onto the surface of materials involved.[47] Among these proteins, fibrinogen, factor IX, prothrombin, factor X, and antithrombin III deserve particular interest as key factors in the activation of all humoral blood reactions. The fact that the intrinsic pathway is specifically altered in contrast to the extrinsic mode is not really surprising keeping in mind that more protein factors are involved in the former one. Although it would be valuable to identify the exact nature of the factor(s) involved in the QDs-mediated coagulation inhibition, this mechanistic study was outside of the main focus of our work.

In vitro Cell Imaging

Use of Ag_2S-DMSA NIRQDs as optical imaging agents was evaluated as well since such bio-applications are the major motivation behind such particles. Couple of examples found in the literature demonstrated in vitro imaging of cancer cells with Ag_2S NIRQDs emitting in the NIR-I[20] and NIR-II window[12]. Also, in vivo imaging of nude mouse with Ag_2Se NIRQDs[14] and Ag_2S NIRQDs[17] were recently reported. Here, HeLa cells incubated with Ag_2S-DMSA NIRQDs 6h was imaged under fluoresence microscope. These QDs are easily excited at 532 nm which causes a minimal autofluoresence from the cells (Fig. 9a) but allows visualization of a very bright cellular image with a high intensity from QD internalized HeLa cells (Fig. 9b).

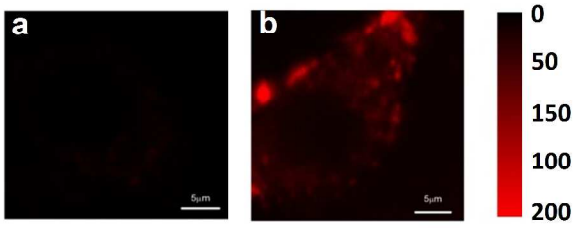

Fig. 9 Fluorescence image of HeLa cells a) without and b) with internalized Ag_2S-DMSA NIRQDs obtained by Confocal laser scanning microscope.

Confocal laser scanning microscope image in Fig. 10 shows strong fluorescence of Ag_2S-DMSA NIRQDs in HeLa cells. These QDs have typical cytoplasmic distribution to endosomes and lysosomes with no nuclear uptake.

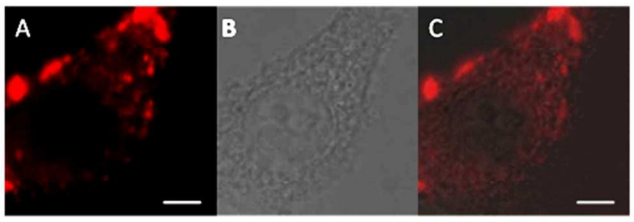

Fig. 10 Cellular uptake and localization of Ag_2S-DMSA NIRQDs by HeLa cells (150 µg/mL QDs, 6h incubation).(A) Fluorescence, (B) Transmission and (C) Overlay channels of confocal micrograph. Scale bar represents 5µm.

Conclusions

In vivo utilization of QDs as imaging agents and/or delivery vehicles require a delicate balance of toxicity, biocompatability, stability, luminescence quality, size and excitation/emission wavelengths. Considering all these Ag_2S NIRQDs present a great potential. Utilization of DMSA, FDA approved heavy metal chelating drug, as a coating and slow sulphur releasing agent under appropriate conditions (pH 7.5 and 70°C and above) provided Ag_2S QDs with tunable emission between 730-900 nm with the best quality particles around 800-860 nm range which is the desired window for medical purposes. QY of these particles are as high as 6.5% and high enough for effective optical imaging. They are demonstrated as effective cytoplasmic imaging agents in HeLa cells. Recently, aqueous Ag_2S QDs coated with BSA were prepared with tunable sizes (within a range of 150 nm)

in the second NIR region with the best particles emitting at around 1150 nm with 1.8% QY[21]. Considering the imaging devices and routine instrumentation, working in the second NIR window is difficult since it is beyond the limits of most widely used Si and PMT detectors.

DMSA coated Ag_2S NIRQDs showed good cytocompatability and hemocompatibility in the *in vitro* experiments without any PEGylation or protein shell such as BSA. This achievement is significant and very valuable for *in vivo* experiments where long blood circulation time and high level of cytocompatibility is necessary. These QDs do not affect the integrity of erythrocytes, do not interact with platelets and show only a slight alteration on the complement system and on the intrinsic pathway of coagulation. To the best of our knowledge this is the first report assessing the hemocompatability of Ag_2S QDs in such detail. Drugs and targeting moieties can be conjugated to the surface carboxylates of these QDs. These NIR QDs hold great potential as new theranostic nanoparticles.

Acknowledgement

Ch. Sevrin has received the financial support of BioMiMedics, an Interreg Project. We would like to thank Dr. Ugur Unal and Cansu Yildirim (KUYTAM, Koc University, Istanbul-Turkey) for XPS and XRD analyses and Dr. Mehmet Ali Gulgun and Melike Yildizhan at SUNUM (Sabanci University, Istanbul-Turkey) for the TEM analysis.

Notes and references

[a]*Koc University, Graduate School of Materials Science and Engineering, Rumelifeneri Yolu, Sarıyer, 34450, Istanbul, Turkey. Fax: +90 2123381559; Tel: +902123381742; E-mail: fyagci@ku.edu.tr.*
[b]*Koc University, Department of Chemistry, Rumelifeneri Yolu, Sarıyer, 34450, Istanbul, Turkey.*
[c]*KUYTAM, Koc University Surface Science and Technology Center, Rumelifeneri Yolu, Sarıyer, 34450, Istanbul, Turkey.*
[d]*Koc University, Department of Physics, Rumelifeneri Yolu, Sarıyer, 34450, Istanbul, Turkey.*
[e]*Centre Interfacultaire des Biomatériaux (CEIB), University of Liège (ULg), Chemistry Institute, B6c, Allée du 6 août, 11, B-4000 Liège (Sart-Tilman), Belgium*

† Electronic Supplementary Information (ESI) available: [details of any supplementary information available should be included here]. See DOI: 10.1039/b000000x/

‡ Footnotes should appear here. These might include comments relevant to but not central to the matter under discussion, limited experimental and spectral data, and crystallographic data.

1. R. Aswathy, Y. Yoshida, T. Maekawa and D. Kumar, *Analytical and Bioanalytical Chemistry*, 2010, 397, 1417-1435.
2. P. P. Ghoroghchian, M. J. Therien and D. A. Hammer, *Wiley Interdisciplinary Reviews: Nanomedicine and Nanobiotechnology*, 2009, 1, 156-167.
3. H. Y. Chen, S. S. Cui, Z. Z. Tu, J. Z. Ji, J. Zhang and Y. Q. Gu, *Photochemistry and Photobiology*, 2011, 87, 72-81.
4. B. Blackman, D. Battaglia and X. Peng, *Chemistry of Materials*, 2008, 20, 4847-4853.
5. S. B. Rizvi, S. Ghaderi, M. Keshtgar and A. M. Seifalian, *Semiconductor quantum dots as fluorescent probes for in vitro and in vivo bio-molecular and cellular imaging*, 2010.
6. A. Guchhait, A. K. Rath and A. J. Pal, *Solar Energy Materials and Solar Cells*, 2011, 95, 651-656.
7. H. Ding, K.-T. Yong, W.-C. Law, I. Roy, R. Hu, F. Wu, W. Zhao, K. Huang, F. Erogbogbo, E. J. Bergey and P. N. Prasad, *Nanoscale*, 2011, 3, 1813-1822.
8. N. Y. Morgan, S. English, W. Chen, V. Chernomordik, A. Russo, P. D. Smith and A. Gandjbakhche, *Academic Radiology*, 2005, 12, 313-323.
9. Y. He, Y. Zhong, Y. Su, Y. Lu, Z. Jiang, F. Peng, T. Xu, S. Su, Q. Huang, C. Fan and S.-T. Lee, *Angewandte Chemie International Edition*, 2011, 50, 5695-5698.
10. R. Xie, K. Chen, X. Chen and X. Peng, *Nano Research*, 2008, 1, 457-464.
11. G. Chen, F. Tian, Y. Zhang, Y. Zhang, C. Li and Q. Wang, *Advanced Functional Materials*, 2014, 24, 2481-2488.
12. Y. Zhang, G. Hong, Y. Zhang, G. Chen, F. Li, H. Dai and Q. Wang, *ACS Nano*, 2012, 6, 3695-3702.
13. Y. Du, B. Xu, T. Fu, M. Cai, F. Li, Y. Zhang and Q. Wang, *Journal of the American Chemical Society*, 2010, 132, 1470-1471.
14. Y.-P. Gu, R. Cui, Z.-L. Zhang, Z.-X. Xie and D.-W. Pang, *Journal of the American Chemical Society*, 2011, 134, 79-82.
15. P. Jiang, Z.-Q. Tian, C.-N. Zhu, Z.-L. Zhang and D.-W. Pang, *Chemistry of Materials*, 2011, 24, 3-5.
16. M. Yarema, S. Pichler, M. Sytnyk, R. Seyrkammer, R. T. Lechner, G. Fritz-Popovski, D. Jarzab, K. Szendrei, R. Resel, O. Korovyanko, M. A. Loi, O. Paris, G. n. Hesser and W. Heiss, *ACS Nano*, 2011, 5, 3758-3765.
17. P. Jiang, C.-N. Zhu, Z.-L. Zhang, Z.-Q. Tian and D.-W. Pang, *Biomaterials*, 2012, 33, 5130-5135.
18. K. P. Remya, T. Udayabhaskararao and T. Pradeep, *The Journal of Physical Chemistry C*, 2012, 116, 26019-26026.
19. G. A. Martínez-Castañón, M. G. Sánchez-Loredo, H. J. Dorantes, J. R. Martínez-Mendoza, G. Ortega-Zarzosa and F. Ruiz, *Materials Letters*, 2005, 59, 529-534.
20. I. Hocaoglu, M. N. Cizmeciyan, R. Erdem, C. Ozen, A. Kurt, A. Sennaroglu and H. Y. Acar, *Journal of Materials Chemistry*, 2012, 22, 14674-14681.
21. Y. Hua-Yan, Z. Yu-Wei, Z. Zheng-Yong, X. Huan-Ming and Y. Shao-Ning, *Nanotechnology*, 2013, 24, 055706.
22. L. Tan, A. Wan and H. Li, *ACS Applied Materials & Interfaces*, 2013, 6, 18-23.
23. R. Gui, A. Wan, X. Liu, W. Yuan and H. Jin, *Nanoscale*, 2014, 6, 5467-5473.
24. E. Sevinc, F. S. Ertas, G. Ulusoy, C. Ozen and H. Y. Acar, *Journal of Materials Chemistry*, 2012, 22, 5137-5144.
25. W. Yantasee, K. Hongsirikarn, C. L. Warner, D. Choi, T. Sangvanich, M. B. Toloczko, M. G. Warner, G. E. Fryxell, R. S. Addleman and C. Timchalk, *Analyst*, 2008, 133, 348-355.
26. J. H. Graziano, N. J. Lolacono, T. Moulton, M. Ellen Mitchell, V. Slavkovich and C. Zarate, *The Journal of Pediatrics*, 1992, 120, 133-139.
27. C. V. Durgadas, K. Sreenivasan and C. P. Sharma, *Biomaterials*, 2012, 33, 6420-6429.

28. D. Painuly, A. Bhatt and V. K. Krishnan, *Journal of Biomaterials Applications*, 2014, 28, 1125-1137.
29. C. V. Durgadas, C. P. Sharma and K. Sreenivasan, *Nanoscale*, 2011, 3, 4780-4787.
30. L. E. Brus, *The Journal of Chemical Physics*, 1984, 80, 4403-4409.
31. L. Brus, *The Journal of Physical Chemistry*, 1986, 90, 2555-2560.
32. S. H. Ehrlich, *Journal of Imaging Science and Technology*, 1993, 37, 73-91.
33. A Guide to Recording Fluorescence Quantum Yields http://www.horiba.com/fileadmin/uploads/Scientific/Documents/Fluorescence/quantumyieldstrad.pdf.
34. S. Celebi, A. K. Erdamar, A. Sennaroglu, A. Kurt and H. Y. Acar, *The Journal of Physical Chemistry B*, 2007, 111, 12668-12675.
35. W. Y. S. Hui Li, Wei-Heng Shih*, *Ind. Eng. Chem. Res.* , 2007, 46, 2013-2019.
36. *Standard X-Ray Diffraction Patterns*, Natl. Bur. Stand. (U.S.), Circ. 539, 1960.
37. O. Madelung, Springer, Verlag Berlin Heidelberg Newyork, 3rd edition edn., 2004, p. 1528.
38. Y. Zhang, Y. Liu, C. Li, X. Chen and Q. Wang, *The Journal of Physical Chemistry C*, 2014, 118, 4918-4923.
39. Handbook of The Elements and Native Oxides, http://www.xpsdata.com/XI_BE_Lookup_table.pdf.
40. R. B. C. Orléans, http://www.lasurface.com/database/elementxps.php.
41. R. Xing, S. Liu and S. Tian, *Journal of Nanoparticle Research*, 2011, DOI: 10.1007/s11051-011-0462-4, 4847-4854.
42. Y. Zhao and Z. Song, *Materials Letters*, 2014, 126, 78-80.
43. C. Grandfils, P. Foresto, B. Riquelme, J. Valverde and D. Sondag-Thull, *Journal of Biomedical Materials Research Part A*, 2008, 84A, 535-544.
44. A. Radomski, P. Jurasz, D. Alonso-Escolano, M. Drews, M. Morandi, T. Malinski and M. W. Radomski, *British Journal of Pharmacology*, 2005, 146, 882-893.
45. D. S. R. Paul M Knopf, Si-Han Hai, Julie McMurry, William Martin and Anne S De Groot, *Immunol Cell Biol*, 2008, 86, 4.
46. M. B. Gorbet and M. V. Sefton, *Biomaterials*, 2004, 25, 5681-5703.
47. B. I. Cerda-Cristerna, H. Flores, A. Pozos-Guillén, E. Pérez, C. Sevrin and C. Grandfils, *Journal of Controlled Release*, 2011, 153, 269-277.